

Genetically-encoded targeted protein degradation technology to remove endogenous condensation-prone proteins and improve crop performance

Received: 13 September 2024

Accepted: 22 January 2025

Published online: 29 January 2025



Ming Luo^{1,2,3}, Sitao Zhu^{1,2,3}, Hua Dang^{1,2,3}, Qing Wen^{1,2,3}, Ruixia Niu^{1,2,3},
Jiawei Long^{1,2,3}, Zhao Wang^{1,2,3}, Yongjia Tong¹, Yuese Ning⁴, Meng Yuan^{2,5} &
Guoyong Xu^{1,2,3} ✉

Effective modulation of gene expression in plants is achievable through tools like CRISPR and RNA interference, yet methods for directly modifying endogenous proteins remain lacking. Here, we identify the E3 ubiquitin ligase E3TCD1 and develop a Targeted Condensation-prone-protein Degradation (TCD) strategy. The X-E3TCD1 fusion protein acts as a genetically engineered degrader, selectively targeting endogenous proteins prone to condensation. For example, a transgenic E3TCD1 fusion with Teosinte branched 1 (TB1) degrades the native TB1 protein, resulting in increased tiller numbers in rice. Additionally, conditional degradation of the negative defense regulator Early Flowering 3 via a pathogen-responsive Pro_{TB1}-uORFs_{TB1} cassette enhances rice blast resistance without affecting flowering time in the absence of pathogen. Unlike prevailing targeted protein degradation strategies, the TCD system does not rely on small molecules, antibodies, or genetic knock-in fusion tags, demonstrating its promise as a transgene-based approach for optimizing crop performance.

Modulating gene expression is crucial not only for advancing our basic scientific understanding of gene functions but also for improving crop performance in practical agricultural settings¹. In the context of protein-coding genes, their expression can be regulated at multiple levels: DNA, mRNA, and protein. CRISPR-DNA editing strategies are powerful tools for modifying DNA in crops². These techniques can alter protein-coding sequences, modify epigenetic marks, and regulate the activity of promoters and RNA regulatory elements^{3,4}. Such variations can influence protein sequences and the efficiency of mRNA transcription and translation. Post-transcriptional methods, such as RNA interference (RNAi) and microRNAs, can also modulate at the RNA

level by targeting specific mRNA for degradation or translational inhibition^{5,6}. Together, these well-established genetic engineering techniques at both the DNA and RNA levels enable quantitative and qualitative control of protein synthesis, a fundamental aspect of proteostasis that occurs at the very beginning of protein formation. Currently, tools directly targeting proteins in plants remain largely unexplored, particularly those aimed at modifying endogenous proteins.

Beyond protein synthesis, plants also regulate proteostasis through additional layers, including modification, trafficking, localization, and degradation. Recent studies highlight the importance of

¹State Key Laboratory of Hybrid Rice, Institute for Advanced Studies (IAS), Wuhan University, Wuhan, Hubei, China. ²Hubei Hongshan Laboratory, Wuhan, Hubei, China. ³RNA Institute, Wuhan University, Wuhan, Hubei, China. ⁴State Key Laboratory for Biology of Plant Diseases and Insect Pests, Institute of Plant Protection, Chinese Academy of Agricultural Sciences, Beijing, China. ⁵National Key Laboratory of Crop Genetic Improvement, National Centre of Plant Gene Research (Wuhan), Huazhong Agricultural University, Wuhan, Hubei, China. ✉e-mail: guoyong.xu@whu.edu.cn

protein condensation through phase separation and transition as a critical layer in proteostasis regulation^{7–13}. This process plays a significant role in shaping plant development and responding to environmental stressors^{14–35}. Homeostasis of all proteins, including condensation-prone ones, is largely regulated by the protein degradation machinery, primarily the ubiquitin-proteasome system (UPS) and the autophagy system^{35–38}. The UPS system operates through the coordinated actions of E1 activating enzymes, E2 conjugating enzymes, and E3 ligases to transfer ubiquitin to the substrate. This often results in polyubiquitylation that targets the substrate for degradation by the proteasome³⁹. The autophagy system, on the other hand, is responsible for degrading not only proteins but also organelles, thus maintaining cellular homeostasis⁴⁰.

Available tools directly shaping proteostasis primarily focus on targeted protein degradation through the UPS and autophagy pathways, which have proven invaluable in human basic research and drug discovery^{41–44}. These targeted protein degradation strategies typically involve the discovery or design of degraders that selectively direct target proteins to the degradation machinery, facilitating their controlled degradation. The degrader plays a central role in mediating the recognition between the target protein and the degradation machinery. Degraders can be small molecules, such as monovalent molecular glues and bifunctional proteolysis-targeting chimeras (PROTACs), or macromolecular conjugates, such as modified antibodies. These strategies can be categorized into two groups based on whether they require a tag fusion to the target protein: genetic-fusion-dependent and genetic-fusion-independent. Dependent strategies require the fusion of a tag sequence to the target protein to be recognized by the degrader, whereas independent strategies primarily rely on specified degraders of small molecules or engineered antibodies to identify and interact with the target. Genetic-fusion-dependent strategies have been introduced in plants and show promise for basic research applications. These strategies include the fusion of various recognizable tags, such as the FKBP destabilizing domain in the shield strategy⁴⁵, the temperature-responsive degron used in the low-temperature degron strategy⁴⁶, GFP or GFP-derivatives utilized in the deGradFP strategy^{47–49}, and the HR1b domain of human PKN1 employed in the E3-DART strategy⁵⁰.

However, applying these strategies in agriculture faces challenges, as they often depend on small chemical molecules, antibodies, or the genetic knock-in of degron sequences fused to endogenous proteins, making them time-intensive and costly. Thus, there is a critical need to develop a straightforward and effective method for directly modifying endogenous plant proteins, enabling advancements in fundamental research and practical agricultural applications. Such an approach could facilitate the rapid genetic improvement of crop performance, aligning with the broader objectives of sustainable agriculture.

In this work, we address these demands by developing the Targeted Condensation-prone-protein Degradation (TCD) strategy. We demonstrate its effectiveness in regulating rice tiller number and flowering. By incorporating a transcriptional and translational control cassette, we are able to boost rice blast resistance while minimizing any negative impact on other growth traits.

Results

Designing the TCD system

A hallmark of protein condensation is the remarkable phenomenon of large-scale coalescence, where identical molecules come together from the soluble phase to form smaller-sized complexes and larger-sized condensates^{10,51,52}. Leveraging this mechanism, we propose fusing the endogenous target protein X with an E3 ligase from the UPS system to generate a genetically engineered protein degrader (X–E3). We hypothesize that X–E3 functions as a bifunctional degrader: on the one hand, it mimics the target protein X to integrate into X-containing

condensates; on the other, it recruits these condensates to the degradation machinery via its E3 ligase function, thereby triggering efficient degradation (Fig. 1a). We opted for Really Interesting New Gene (RING) E3 ubiquitin ligases for their prominence as the largest family in plants and their ability to act as both multimeric and monomeric E3 ligases in plant systems^{53,54}. In addition, RING E3 ligases have been extensively used in current targeted protein degradation strategies in animals. Given that each plant species contains hundreds of RING E3 ligases (Supplementary Data 1), we refined our focus to those that are intrinsically disordered proteins (IDPs) with low-complexity domains (LCD) which is a good predictor for condensation. Since these domains are often sufficient to promote heterogeneous protein condensation upon fusion^{10,51,52}, we hypothesized that the E3 LCD domains in the degrader could facilitate protein degradation. Before supporting this hypothesis, we faced the immediate question of identifying RING E3 ligases with condensation capacity.

Screening E3 with condensation capacity

We predicted 51 out of 508 possible RING E3 in *Arabidopsis* as IDPs (E3IDP1–51) using the PLAAC algorithm⁵⁵. These E3IDPs also show high potential to be IDPs, as predicted by the Molecular Condensation and Phase Separation Predictor⁵⁶. We successfully cloned 44 for further screening (Fig. 1b and Supplementary Data 2). As protein concentration increases, it promotes protein condensation⁵². Therefore, we overexpressed these proteins tagged with the yellow fluorescence protein (E3IDP–YFP) in *N. benthamiana* to determine their condensation behaviors. We discovered that 17 RING E3 proteins formed visible condensates (e.g., E3IDP1), while 17 did not (e.g., E3IDP6; Fig. 1b, c). Surprisingly, ten E3 ligases did not show obvious YFP signals, but the co-expressed CFP control was always detected in the nucleus (e.g., E3IDP8 and E3IDP45; Fig. 1b, d).

We experimented with these ten E3 by deleting the predicted RING domain (E3IDP^{ΔRING}; Supplementary Data 2), which plays a crucial role in recruiting other components of the UPS system. We observed that five E3 ligases failed to generate YFP signals after removing the predicted RING domains (e.g., E3IDP8 vs. E3IDP8^{ΔRING}; Fig. 1d). However, we observed the reappearance of YFP signals as condensates for the remaining five E3 after removing the predicted RING domains (e.g., E3IDP45 vs. E3IDP45^{ΔRING}; Fig. 1d, e). Thus, we identified 17 RING E3 ligases that formed constitutive condensates and 5 that required the removal of the predicted RING domain to condense. The latter group, likely capable of self-recognition and self-degradation, emerges as promising candidates for engineering X–E3 fusions due to their potential to self-degrade and avoid accumulation in cells before or after clearing X-containing condensates.

Characterizing E3IDP45 with condensation capacity

Since these five E3 ligases exhibit similar cellular condensation behavior and share a predicted LCD (Fig. 1e and Supplementary Fig. 1), we selected E3IDP45, for which we have available vectors of domain truncations, to further test its condensation and self-degradation capabilities. We conducted an in vitro analysis of its condensation behavior. We expressed maltose-binding protein (MBP)-tagged YFP–E3IDP45 in *Escherichia coli*. Initially, before removing MBP, we observed that the purified MBP–YFP–E3IDP45 exhibited predominantly spherical droplets with fewer fibrous condensates when exposed to a crowding agent that promotes intermolecular interaction (Supplementary Fig. 2a). However, upon removal of the molecular chaperone MBP, YFP–E3IDP45 underwent a rapid phase transition, resulting in increased turbidity with escalating concentrations of the crowding agent (Supplementary Fig. 2b). Notably, we observed swift formation of non-liquid irregular condensates emerging from the spherical droplets (Supplementary Fig. 2a). These irregular condensates displayed reduced material exchange with the surrounding solution, as evidenced by their slower recovery rate in the fluorescence

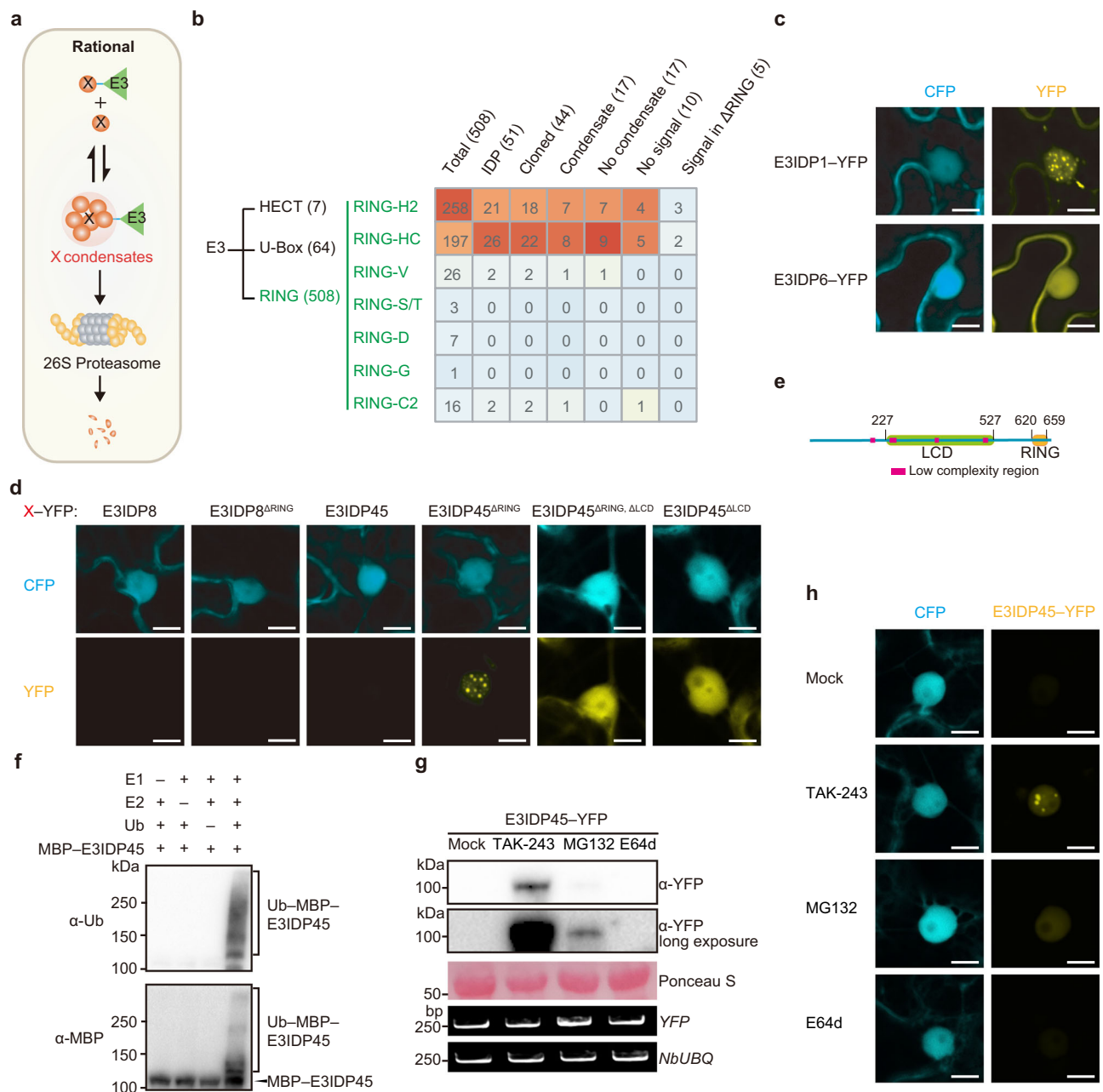


Fig. 1 | Screening E3 ligases with condensation and self-degradation capacities for the Targeted Condensation-prone Protein Degradation system (TCD). See also Supplementary Figs. 1, 2. **a** The schematic diagram of TCD. X, an endogenous target protein. E3, an E3 ligase from the UPS system. X-E3, a genetically engineered protein degrader by fusing X with E3. **b** The heatmap to show the distribution of E3 ligases among the RING subfamilies during screening. Plants possess three families of E3 ligases: RING, HECT, and U-box. A total of 508 RING E3 ligases were analyzed using PLAAC to predict their status as intrinsically disordered proteins (IDPs). Of these, 51 were identified as potential IDPs (E3IDPs). Among these E3IDPs, 44 were successfully cloned and expressed in *N. benthamiana* as YFP fusion proteins (E3IDP-YFP). 17 E3IDPs formed visible condensates, 17 did not form visible condensates, and 10 exhibited no detectable fluorescence signals. Deleting the RING domain (ΔRING) restored YFP fluorescence as condensates for five of the ten fluorescenceless E3IDP-YFP. **c** Exemplifying E3IDPs with (E3IDP1) or without

(E3IDP6) visible condensates. **d** Exemplifying E3IDPs with or without RING domains (ΔRING). ΔLCD, deleting the LCD domain. **e** The domain organization of E3IDP45. The SMART website predicts low-complexity regions (red) and the RING domain (orange; 620–659). LCD, the truncation-experiment-mapped region (green; 227–527) required to form visible condensates in *N. benthamiana*. **f** In vitro ubiquitination assay to evaluate the self-ubiquitination capacity of E3IDP45. E1, E2, and ubiquitin (Ub) are components of the ubiquitin-transfer cascade with MBP-tagged E3IDP45 (MBP-E3IDP45) simultaneously as an E3 and substrate. **g, h** Immunoblot analysis (**g**) and microscopic observation (**h**) of E3IDP45-YFP in the absence (Mock) or presence of E1 inhibitor TAK-243, the proteasome inhibitor MG-132, and the autophagy inhibitor E64d. Ponceau S staining (**g**) was used as a control for protein loading. Semi-quantitative RT-PCR was conducted against YFP with *NbUBQ* as the internal control (**g**). For microscopic observation, 35S::CFP serves as the control (**c, d, h**). Scale bar, 10 μm (**c, d, h**). Source data are provided as a Source Data file.

recovery after photobleaching (FRAP) assay compared to those formed by MBP-YFP-E3IDP45 (Supplementary Fig. 2c). In addition, they resisted dissolution by high concentrations of salt or 1,6-hexanediol, which disrupt molecular interactions (Supplementary Fig. 2d).

Thus, our findings indicate that E3IDP45 exhibits a high propensity for condensation in vitro.

We then conducted an in vivo analysis of its condensation behavior using E3IDP45^{ΔRING} because the full length was not stable in plants

(Fig. 1d). Upon transient expression in *N. benthamiana*, we observed the fusion behavior among the E3IDP45^{ARING} condensates (Supplementary Fig. 2e). Furthermore, FRAP revealed consistent interchangeability of these condensates with the surrounding soluble fractions (Supplementary Fig. 2f, g). However, the slow recovery efficiency suggests these condensates are more densely packed. Furthermore, these condensates remained unaffected by the dissolving agent 1,6-hexanediol (Supplementary Fig. 2h). To investigate whether E3IDP45^{ARING} condensation responds to environmental stressors, we applied one biotic stressor (salicylic acid) and three abiotic stressors (cold, heat, and osmosis). Among these, only heat treatment induced the formation of larger condensates, while the condensates remained unchanged under other conditions (Supplementary Fig. 2h). We then performed truncation assays based on E3IDP45^{ARING} and found that amino acids from 227–527, which contains the predicted LCD, is necessary and sufficient to detect visible E3IDP45^{ARING} condensates (Supplementary Fig. 2i). Thus, we could not detect visible condensates after removing this region in E3IDP45^{ARING} (E3IDP45^{ARING, ΔLCD}; Fig. 1d, e). As we focused on utilizing these E3IDPs for engineering purposes, we did not assess their potential for condensation at the natural expression level using the native promoters. Nevertheless, these results suggest that E3IDP45^{ARING} undergoes strong and stable condensation, warranting further characterization to explore its dynamic behavior over time and under varying intensities of diverse stressors.

Characterizing E3IDP45 with self-degradation capacity

We then performed an in vitro ubiquitination assay to evaluate the self-degradation capacity of E3IDP45. Immunoblot analysis revealed that polyubiquitination of MBP-tagged E3IDP45 (MBP–E3IDP45) occurred only in the presence of all components of the ubiquitin-transfer cascade (E1, E2, and ubiquitin). This was evidenced by detecting a slow-migrating ladder on gels probed with antibodies against ubiquitin and the MBP tag, indicating that E3IDP45 can ubiquitinate itself in vitro (Fig. 1f).

To determine whether the lack of detectable E3IDP45–YFP signal in vivo was due to self-degradation, we inhibited major degradation pathways in *N. benthamiana*. Using the E1 inhibitor TAK-243, the proteasome inhibitor MG-132, and the autophagy inhibitor E64d, we assessed E3IDP45–YFP protein levels. TAK-243 significantly increased E3IDP45–YFP levels from undetectable levels in the mock control, while E64d showed no effect. MG-132 produced only a modest increase in protein levels, potentially due to differences in inhibitory efficiency, concentration, or treatment time (Fig. 1g). Both TAK-243 and MG-132 treatments restored confocal signals, although visible condensates were observed only with TAK-243, aligning with immunoblot results that TAK-243 accumulated more protein for condensation (Fig. 1h). We also showed that removing the LCD domain in the presence of the RING domain resulted in high fluorescence intensity without visible condensates, suggesting that condensation is essential for self-degradation (E3IDP45^{ΔLCD}; Fig. 1d). These findings indicate that E3IDP45 recognizes itself as a substrate for degradation and that the LCD domain is crucial for efficient self-degradation, highlighting its potential as a strong candidate for engineering the TCD system.

Testing the TCD system with E3IDP45

To validate the TCD system, we designed rapid transient experiments involving microscopic observation and immunoblot analysis to test whether the X–E3 degrader could efficiently degrade the target X protein (Fig. 2a). We first implemented the TCD experimental setup using E3IDP45^{ARING} as the X protein to examine whether E3IDP45 could act as a degrader to eliminate E3IDP45^{ARING}. Once again, we failed to detect E3IDP45–YFP through microscopic observation or immunoblot analysis (Fig. 2b, c). Subsequently, we expressed E3IDP45^{ARING}–YFP and observed the re-emergence of condensates in the nucleus (Fig. 2b). Remarkably, co-expression of the full-length E3IDP45 as the X–E3

degrader effectively diminished these E3IDP45^{ARING}–YFP condensates (Fig. 2b). Immunoblot analysis confirmed the depletion of E3IDP45^{ARING}–YFP at the protein level, while their mRNA levels remained consistent regardless of co-expression with E3IDP45 (Fig. 2c).

To further validate the TCD system, we focused on two key questions: First, can fusing E3IDP45 with various X proteins effectively induce their degradation? Second, is this degradation specific to the X proteins? For the first question, we specifically chose transcription factors (TFs) for examination due to mounting evidence across animal and plant studies indicating that TFs and their regulators form biomolecular condensates to regulate transcription^{14,16,23,31,32,57–61}. We fused E3IDP45 to eight TFs from the TCP, AP2, bZIP, ZnF, and NAC families of rice as degraders (Supplementary Data 3), which were co-expressed with their corresponding TF–YFP as targets in *N. benthamiana*. Our findings revealed that six of the TF–E3IDP45 degraders were capable of degrading their respective TF–YFP target, as indicated by reduced fluorescence (PLP20/139/165/187/206/308; Supplementary Fig. 3a). We successfully conducted immunoblot analysis on six out of the eight TF–YFP samples and found results consistent with our fluorescence observations (five shown in Supplementary Fig. 3b with PLP308 shown below).

In addition, we noted that the TCD mechanism was effective not only in degrading proteins capable of forming visible condensates (PLP20/165/206/308) but also in those existing in the soluble fraction (PLP139/187). Given that all TFs are predicted to possess disordered regions (Supplementary Fig. 3c), it is plausible that the diffused TFs may cluster in sizes below the detection limit or necessitate additional stimulating conditions for visible condensate formation^{13,16,17}. Notably, two TFs were not efficiently degraded in these assays (PLP32/247; Supplementary Fig. 3a). While the exact system requirements for effectiveness were not fully established, we strongly recommend rapid pilot experiments before subsequent studies (Fig. 2a).

For the second question, we tested each TF–E3IDP45 degrader for the six TF–YFP targets and revealed selective degradation of the corresponding target only (Fig. 2d). Immunoblot analysis further confirmed that E3IDP45^{ARING}–YFP and PLP308–YFP was exclusively degraded by their corresponding degraders, E3IDP45 and PLP308–E3IDP45, respectively, and not by other TF–E3IDP45 degraders (Fig. 2e, f). While these results are robust and suggest that X–E3IDP45 fusions likely do not recognize substrates of E3IDP45, we have not fully explored all possible unidentified substrates of E3IDP45. We thus suggest using E3IDP45 as a control in pilot or subsequent comparison experiments (Fig. 2a). These findings highlight the efficiency and specificity of the TCD system in degrading endogenous proteins.

Evaluating the E3IDP45 condensation capacity

To investigate how the condensation capacity influences target degradation, we aimed to remove the LCD domain from either the target or the degrader to determine whether the condensation capacity of E3IDP45 is essential for degradation. Before proceeding, we assessed whether deleting the LCD domain from E3IDP45 would affect its self-interaction. Since E3IDP45 undergoes self-degradation, we performed these experiments using the E3IDP45^{ARING} variant. Co-immunoprecipitation revealed that E3IDP45^{ARING} with the LCD domain deleted (E3IDP45^{ARING, ΔLCD}) could still interact with E3IDP45^{ARING} (Fig. 2g). We next analyzed the role of the LCD domain in target X by reducing its condensation capacity through deletion of the LCD domain (E3IDP45^{ARING, ΔLCD}) while retaining this capacity in the co-expressed E3IDP45 degrader. Our results showed that the soluble form of E3IDP45^{ARING, ΔLCD}–YFP could not be efficiently degraded by E3IDP45 (Fig. 2h, i). Similarly, truncation assays on PLP308–YFP revealed that only truncations showing visible condensates correlated with high degradation efficiency by the degrader

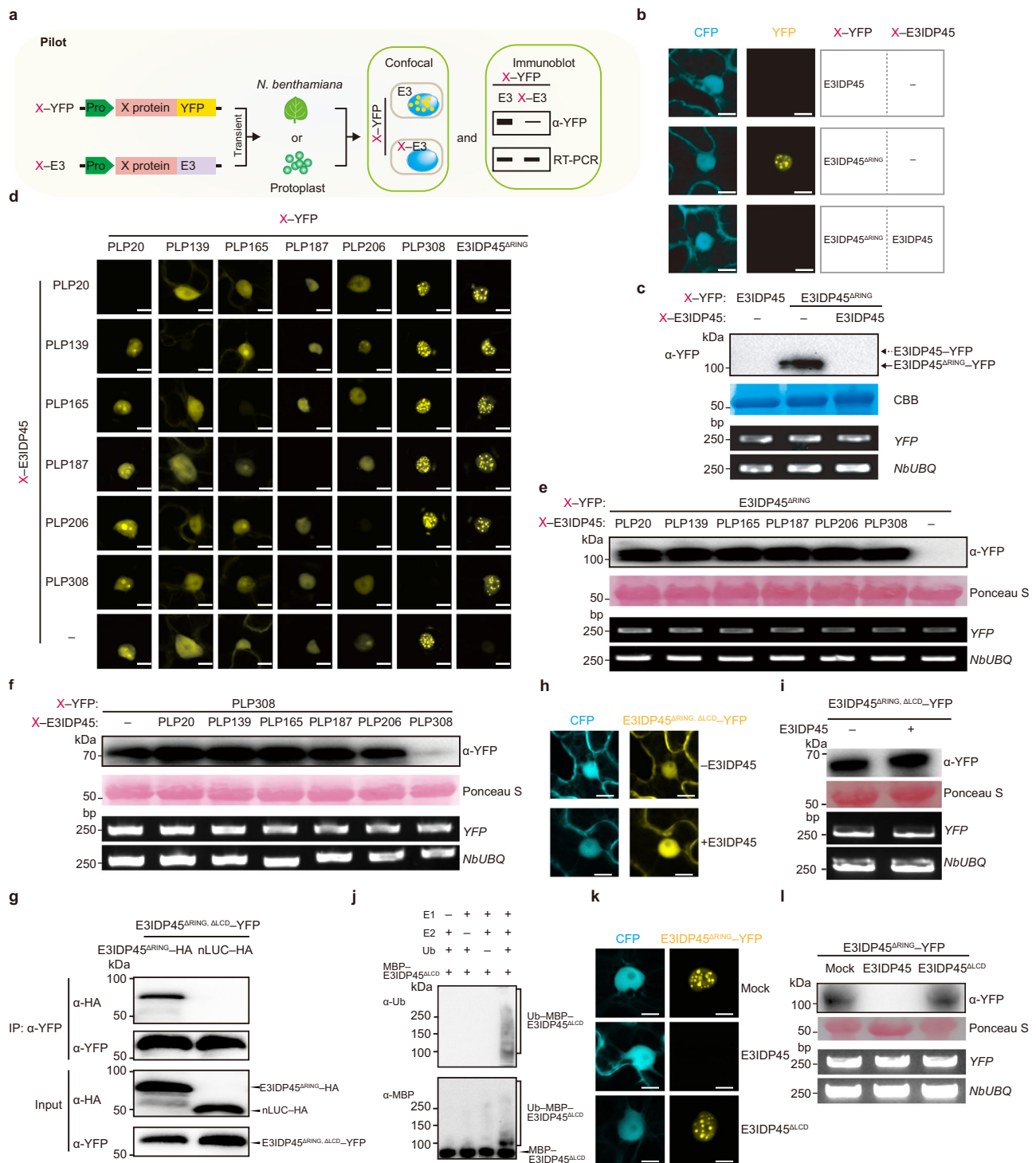


Fig. 2 | Validating E3IDP45 for the TCD system. See also Supplementary Figs. 3, 4. **a** The schematic of the pilot assays involving transient expression of the X-E3 degrader with the X-YFP target in *N. benthamiana* or protoplasts to assess TCD efficiency via microscopic observation or immunoblot analysis. X-YFP, YFP-tagged target protein X. X-E3, the degrader for X after fusing with E3. **b, c** Degradation of the E3IDP45^{ΔRING}-YFP by the E3IDP45 degrader in the pilot experiments of microscopic observation (**b**) and immunoblot analysis (**c**) in *N. benthamiana*. **d** Microscopic observation of each X-YFP after co-expression with different X-E3IDP45 degraders. Six transcription factors and the E3IDP45^{ΔRING} were examined as the target X protein. **e, f** Immunoblot analysis of E3IDP45^{ΔRING}-YFP (**e**) and PLP308-YFP (**f**) after co-expression with different X-E3IDP45 degraders. **g** Co-immunoprecipitation to show the interaction between E3IDP45^{ΔRING} with the LCD

domain deleted (E3IDP45^{ΔRING, ΔLCD}) and E3IDP45^{ΔRING}. **h, i** Degradation of E3IDP45^{ΔRING}-YFP without the LCD in the target (E3IDP45^{ΔRING, ΔLCD}) by the E3IDP45 degrader in the pilot experiments of microscopic observation (**h**) and immunoblot analysis (**i**) in *N. benthamiana*. **j** In vitro ubiquitination assay to evaluate the self-ubiquitination capacity of E3IDP45^{ΔRING}. **k, l** Degradation of the E3IDP45^{ΔRING}-YFP target by degraders of E3IDP45 without the LCD in the degrader (E3IDP45^{ΔLCD}) in the pilot experiments of microscopic observation (**k**) and immunoblot analysis (**l**) in *N. benthamiana*. Coomassie brilliant blue (CBB; **c**) or Ponceau S staining (**e, f, i, l**) was used as a control for protein loading. Semi-quantitative RT-PCR was conducted against YFP with *NbUBQ* as the internal control (**c, e, f, i, l**). For microscopic observation, 35S::CFP serves as the control (**b, h, k**). Scale bar, 10 μm (**b, d, h, k**). Source data are provided as a Source Data file.

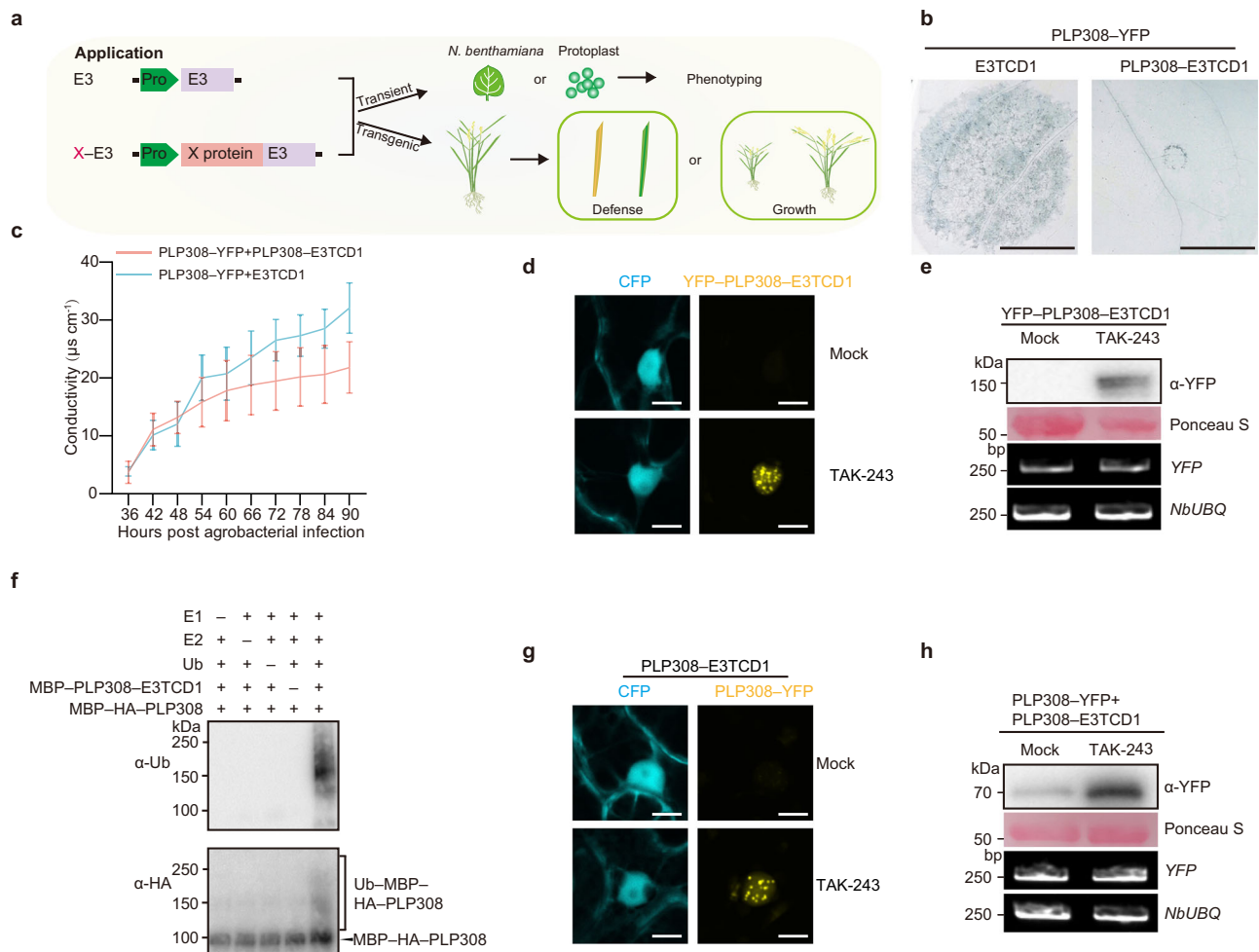


Fig. 3 | Genetic analysis of PLP308 in promoting cell death by the TCD via the transient assay. See also Supplementary Fig. 5. **a** The schematic to illustrate the application of the TCD system for genetic analysis of target protein X through transient and transgenic assays. Different promoters (Pro) are necessary to control the spatial and temporal expression as well as the expression intensity of the degrader X-E3. **b** Trypan blue staining to show PLP308-YFP-triggered cell death without (E3TCD1) or with the degrader (PLP308-E3TCD1). Macroscopic cell death appears after transient expression of PLP308-YFP in *N. benthamiana* for 72 h. **c** Ion leakage to show PLP308-YFP-triggered cell death. Leaf discs were used for measuring ion leakage after transient expression of PLP308-YFP in *N. benthamiana*. The points and error bars show the mean \pm s.d. of ion concentration ($n = 4$; 6 discs each). **d, e** Microscopic observation (**d**) and immunoblot analysis (**e**) of the YFP-tagged PLP308-E3TCD1 degrader (YFP-PLP308-E3TCD1) in the absence (Mock) or

presence of E1 inhibitor TAK-243 after transient expression in *N. benthamiana*. **f** In vitro ubiquitination assay to detect the ubiquitination of the target PLP308 by the degrader PLP308-E3TCD1. E1, E2, and ubiquitin (Ub) are components of the ubiquitin-transfer cascade with MBP-tagged PLP308-E3TCD1 (MBP-PLP308-E3TCD1) as an E3 and MBP-HA-PLP308 as a substrate. HA, hemagglutinin tag. **g, h** Microscopic observation (**g**) and immunoblot analysis (**h**) of the PLP308-YFP degradation by the PLP308-E3TCD1 degrader in the absence (Mock) or presence of E1 inhibitor TAK-243 after transient expression in *N. benthamiana*. Ponceau S staining (**e, h**) was used as a control for protein loading. Semi-quantitative RT-PCR was conducted against YFP with *NbUBQ* as the internal control (**e, h**). For microscopic observation, 35S::CFP serves as the control (**d, g**). Scale bar, 1 cm (**b**), 10 μ m (**d, g**). Source data are provided as a Source Data file.

PLP308-E3IDP45. In contrast, the fragment comprising amino acids 301–423, which exhibited a soluble distribution in the nucleoplasm and nucleus, was not degraded (Supplementary Fig. 4a, b). These findings suggest that the condensation behavior of the target is critical for efficient degradation.

We further investigated the role of the degrader's condensation behavior. An in vitro ubiquitination assay revealed that deleting the LCD domain from the E3IDP45 degrader (E3IDP45^{ΔLCD}) did not impair its self-ubiquitination capacity (Fig. 2j). However, this modification rendered the degrader incapable of efficiently degrading the target E3IDP45^{ΔRING}-YFP in plants (Fig. 2k, l). HOS1, a RING E3 ligase with no reported condensation behavior⁶², served as a soluble E3 ligase control. We found that its fusion with the target could not degrade the respective TF-YFP targets (Supplementary Fig. 4c–f). These findings reinforce our initial hypothesis that LCD-mediated condensation of the E3 ligase is essential for effective substrate degradation. To classify E3

ligases compatible with the TCD system, we introduced the suffix E3TCD. Accordingly, E3IDP45 has been renamed as E3TCD1.

Genetic analysis with E3TCD1 (E3IDP45) in the transient assay

We aimed to investigate whether the degradation of endogenous proteins via the TCD system induced any phenotypic changes. To assess the TCD system's impact, we employed both transient and transgenic methods, which are commonly utilized for determining protein functions (Fig. 3a). Our transient experiment focused on PLP308, a rice Zinc-finger TF whose physiological roles remain unknown, as previous assays revealed that prolonged expression of PLP308-YFP induced cell death in *N. benthamiana*. When PLP308-YFP was co-expressed with the control E3TCD1 in *N. benthamiana*, it triggered noticeable macroscopic cell death, evidenced by intensified trypan blue staining and increased ion leakage (Fig. 3b, c). In contrast, since PLP308-YFP is efficiently and specifically degraded by the

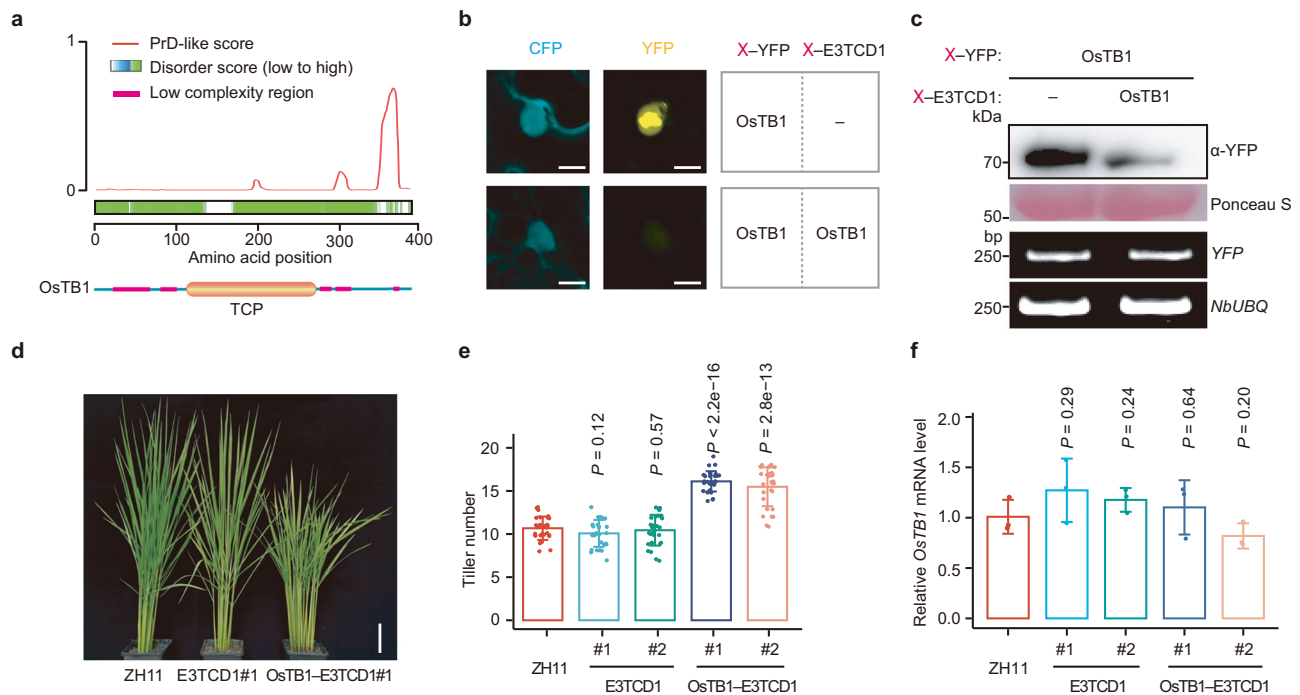


Fig. 4 | Modulating rice tiller numbers by the TCD system in rice. **a** Prediction of OsTB1 as an intrinsically disordered protein (IDP) using PLAAC and D²P² algorithms indicated by Prion domain (PrD)-like score and disorder score, respectively. The bottom section displays low complexity regions and the RING domain as annotated by the SMART website. **b**, **c** Pilot experiments to show the degradation of OsTB1 by the OsTB1-E3TCD1 degrader through microscopic observation (**b**) and immunoblot analysis (**c**). Ponceau S staining was used as a control for protein loading. For microscopic observation, 35S::CFP serves as the control. Semi-quantitative RT-PCR is conducted against YFP with *NbUBQ* as the internal control. **d**, **e** The rice tiller numbers in rice Zhonghua11 (ZH11) plants transformed with 35S::E3TCD1 or

35S::OsTB1-E3TCD1. Two independent transgenic lines (#1 and #2) were used for each construct. The bars show the mean \pm s.d. ($n = 30$) of tiller numbers, and a two-sided Student's *t* test was used to determine the significance. **f** Quantitative RT-PCR to show the relative endogenous *OsTB1* mRNA levels in the transgenic lines. Primers binding to the untranslated region, which was not included in the OsTB1-E3TCD1 transgene, were used to amplify the endogenous *OsTB1* gene. The bars show the mean \pm s.d. ($n = 3$) after normalization to ZH11, a two-sided Student's *t* test was used to determine the significance. Scale bar, 10 μ m (**b**), 10 cm (**d**). Source data are provided as a Source Data file.

degrader PLP308-E3IDP45 (hereafter referred to as PLP308-E3TCD1; Fig. 2b), co-expression with PLP308-E3TCD1 significantly reduced cell death (Fig. 3b, c). This suggests that the TCD system can be utilized in transient expression systems to investigate gene functions by effectively regulating protein levels.

To investigate the mechanism by which the PLP308-E3TCD1 degrader facilitates efficient PLP308 degradation, we first confirmed that PLP308-E3TCD1 underwent self-degradation. Despite adding a YFP tag to the degrader, we failed to detect any fluorescence or immunoblot signals. However, treatment with TAK-243 significantly restored both the fluorescence and immunoblot signals (Fig. 3d, e). We then performed an in vitro ubiquitination assay and found that the substrate MBP-HA-PLP308 exhibited a slow-migrating ladder only in the presence of MBP-E3TCD1-PLP308, along with the necessary components on the gel blotted with anti-HA, suggesting that PLP308-E3TCD1 can ubiquitinate PLP308 in vitro (Fig. 3f). Furthermore, we detected PLP308-YFP signals in the presence of the PLP308-E3TCD1 degrader after TAK-243 treatment, as evidenced by both confocal microscopy and immunoblot analysis (Fig. 3g, h). These results suggest that the PLP308-E3TCD1 degrader can ubiquitinate PLP308, leading to its degradation via the UPS system.

As the co-expression assay primarily reflects the outcome, the observed degradation efficacy might be attributed to the clearance of PLP308-YFP before they reached high expression levels. Consequently, we assessed whether PLP308-E3TCD1 could continue removing PLP308-YFP even after it accumulated to high expression levels and formed extensive condensates. We expressed PLP308-YFP for 48 h and then induced PLP308-E3TCD1 expression using the β -estradiol-inducible system (Supplementary Fig. 5a). Remarkably,

PLP308-E3TCD1 effectively degraded PLP308-YFP condensates even at high expression levels (Supplementary Fig. 5b, c). Furthermore, we found that the UPS system inhibitor, MG132, could inhibit PLP308-E3TCD1-triggered degradation of PLP308-YFP (Supplementary Fig. 5c). This suggests that the PLP308-E3TCD1 degrader initiates the degradation of PLP308-YFP through the TCD, thereby mitigating the associated phenotype.

Genetic analysis with E3TCD1 in the transgenic assay

To evaluate the effect of the TCD system in transgenic plants, our primary focus was on a rice TCP-type TF, Teosinte Branched 1 (OsTB1). This choice was motivated by the apparent phenotype observed in rice with mutations in *OsTB1* DNA, which results in increased tillering numbers^{63–66}. OsTB1 has a predicted IDR with PLAAC (Fig. 4a). We discovered an irregular condensate of OsTB1-YFP in the nucleus, indicating that OsTB1 has the potential to form condensates (Fig. 4b). The pilot experiments showed a decrease in OsTB1-YFP condensates and protein after co-expressing OsTB1-E3TCD1, suggesting that the OsTB1-E3TCD1 degrader can degrade OsTB1 (Fig. 4b, c).

We introduced OsTB1-E3TCD1 (35S::OsTB1-E3TCD1) and the E3TCD1 control (35S::E3TCD1), both driven by the CaMV 35S promoter, into the rice cultivar Zhonghua 11 (ZH11). We found no statistically significant difference in the tillering number between ZH11 and the 35S::E3TCD1 control lines. This suggests that the self-degradation property of E3TCD1 prevents potential negative impacts on plant growth (Fig. 4d, e). The transgenic lines with 35S::OsTB1-E3TCD1 showed increased tillering numbers compared to 35S::E3TCD1, consistent with plants that have the DNA mutation on *OsTB1*, as reported (Fig. 4d, e). We then performed RT-PCR against the untranslated

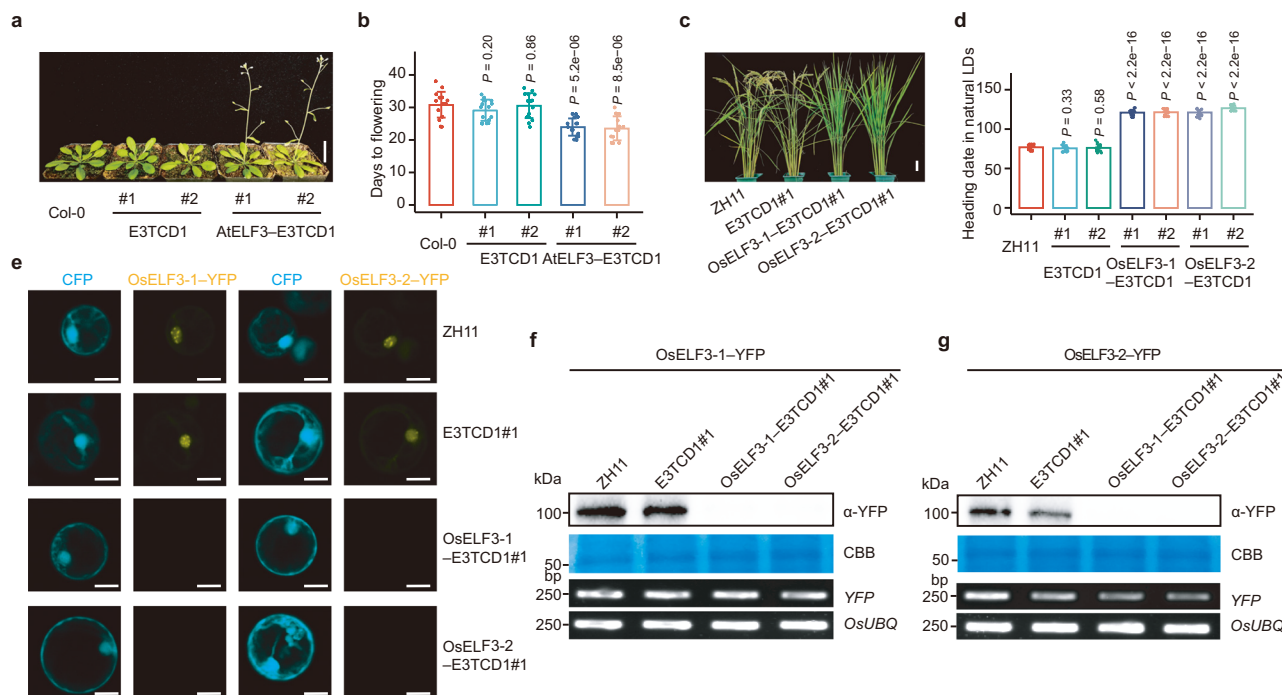


Fig. 5 | Modulating flowering times in *Arabidopsis* and rice with the TCD system. See also Supplementary Figs. 6–9. **a, b** The flowering phenotype of *Arabidopsis* Col-0 plants transformed with 35S::E3TCD1 or 35S::AtELF3–E3TCD1. Two independent transgenic lines (#1 and #2) are shown. The bars show the mean \pm s.d. ($n = 16$) of the days to flowering after seeding, and a two-sided Student's t test was used to determine the significance. **c, d** The flowering phenotype of rice Zhonghui1 (ZH11) plants transformed with 35S::E3TCD1, 35S::OsELF3-1–E3TCD1 or 35S::OsELF3-2–E3TCD1. Two independent transgenic lines (#1 and #2) were used for each construct. The bars show the mean \pm s.d. ($n = 15$) of the days to heading after seeding under the natural long-day (LD) condition, and a two-sided Student's

t test was used to determine the significance. **e–g** In planta degradation assay to demonstrate the degradation of the OsELF3-1 or OsELF3-2 target protein by the OsELF3-1–E3TCD1 or OsELF3-2–E3TCD1 degrader by microscopic observation (**e**) and immunoblot analysis (**f**, OsELF3-1; **g**, OsELF3-2). The plasmids of 35S::CFP/35S::OsELF3-1–YFP or 35S::CFP/35S::OsELF3-2–YFP were co-transformed into the protoplasts prepared from the transgenic plants. Coomassie brilliant blue (CBB) was used as a control for protein loading. Semi-quantitative RT-PCR was conducted against YFP with *NbUBQ* as the internal control. Scale bar, 3 cm (**a**), 10 cm (**c**), 10 μ m (**e**). Source data are provided as a Source Data file.

region, which was not included in the OsTBI–E3TCD1 transgene, and detected similar mRNA levels for the endogenous *OsTBI* gene. This suggests that the phenotype was not caused by potential RNA interference (Fig. 4f). These results suggest that the TCD system can efficiently degrade endogenous proteins and produce desirable traits.

Using the TCD to modulate flowering time

The successful application of TCD in regulating rice tillering underscores the promising potential of this system for optimizing crop performance. Next, we focused on modulating flowering time, known as heading date, a crucial agronomic trait in rice that influences its region adaptation and grain yield. We targeted rice early flowering 3 (ELF3) because its *Arabidopsis* homolog (AtELF3) is a condensation-prone protein involved in transcriptional regulation^{16,67}. The pilot experiment in *N. benthamiana* showed that the AtELF3–E3TCD1 degrader reduced the AtELF3–YFP protein, indicating its potential to degrade endogenous AtELF3 (Supplementary Fig. 6a, b). Again, the control line 35S::E3TCD1 did not negatively impact the plant growth compared to the non-transformed Col-0. However, transgenic plants expressing 35S::AtELF3–E3TCD1 displayed a notable tendency toward early flowering (Fig. 5a, b). This observation aligns with findings from plants harboring mutations in *AtELF3* DNA^{16,67}.

In contrast to the inhibitory role of *Arabidopsis* ELF3, rice has two homologs of ELF3, with OsELF3-1 playing a more dominant role in promoting flowering than OsELF3-2^{68–70}. We showed that both homologs exhibited high sequence similarity (Supplementary Fig. 7a and Supplementary Data 4). We characterized OsELF3-1 in vitro and observed that MBP–YFP–OsELF3-1 did not form condensates even in the presence of a 10% crowding agent. However, after removing the

molecular chaperone MBP, as little as 5% crowding agent was sufficient to induce the formation of large, irregular condensates, which exhibited slow recovery efficiency in FRAP analysis (Supplementary Fig. 7b–d). In vivo FRAP analysis of OsELF3-1's condensation behavior in *N. benthamiana* revealed consistent interchangeability between these condensates and the surrounding soluble fractions. The observed slow recovery efficiency further indicates that these condensates are more densely packed (Supplementary Fig. 7e, f).

The rapid condensation into irregular and solidified structures was also observed for the in vitro purified degrader protein OsELF3-1–E3TCD1, even in the presence of the MBP chaperone (MBP–YFP–OsELF3-1–E3TCD1) (Supplementary Fig. 7g, h). As a control, we induced condensation using the LCD domain found exclusively in plant homologs of Hematopoietic protein 1²⁸. This control formed spherical and phase-separated condensates, suggesting that the rapid condensation behavior is intrinsic to OsELF3-1 itself and not due to the experimental conditions (Supplementary Fig. 7i). In addition, YFP-tagged OsELF3-1–E3TCD1 did not produce detectable fluorescence signals; however, treatment with TAK-243 significantly restored fluorescence, appearing as condensates. FRAP analysis revealed that these condensates displayed consistent, though slower, interchangeability with the surrounding environment (Supplementary Fig. 7j, k). These findings indicate that both OsELF3-1 and its corresponding degrader, OsELF3-1–E3TCD1, can undergo condensation in vitro and in vivo. In addition, the degrader is capable of undergoing self-degradation in vivo.

OsELF3-1 and OsELF3-2 could interact with each other, as evidenced by the split-luciferase complementation assay and co-immunoprecipitation (Supplementary Fig. 8a, b). Furthermore, the

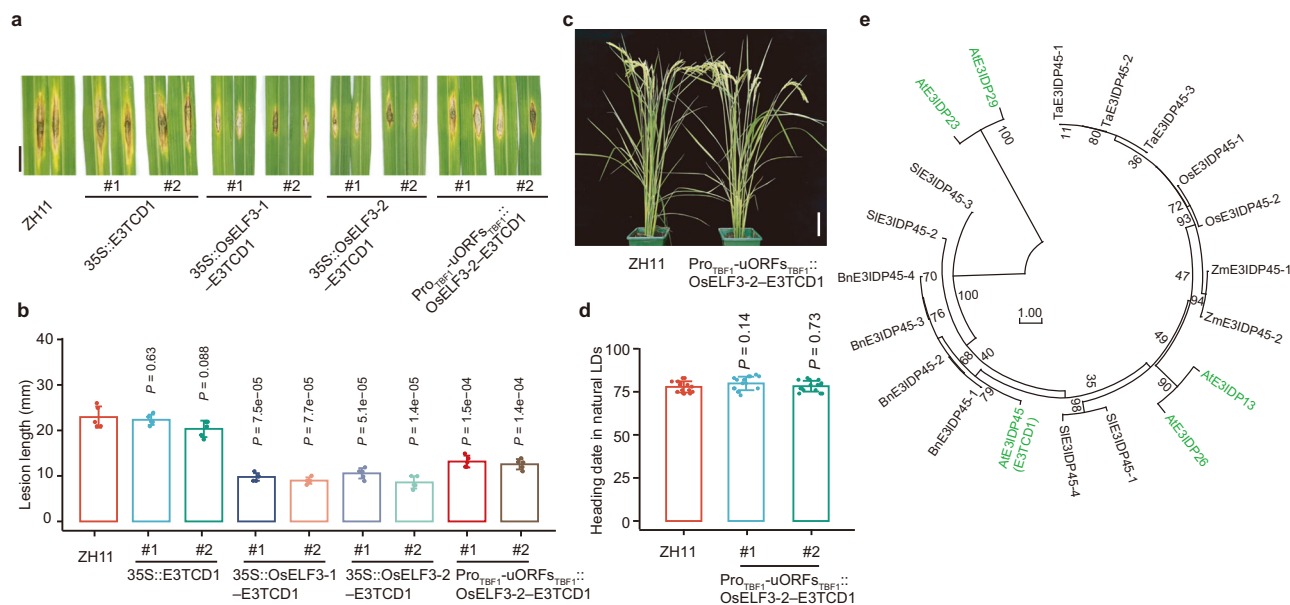


Fig. 6 | Conditional TCD with the TBF1 expression control cassette. See also Supplementary Fig. 8. **a, b** Symptoms and quantification after the fungal pathogen *M. oryzae* infection in the growth chamber on rice Zhonghua11 (ZH11) plants transformed with 35S::E3TCD1, 35S::OsELF3-1-E3TCD1, 35S::OsELF3-2-E3TCD1 or Pro_{TBF1}-uORFs_{TBF1}::OsELF3-2-E3TCD1. Two independent transgenic lines (#1 and #2) were used for each construct. Pro_{TBF1}-uORFs_{TBF1}, the ‘TBF1-cassette’ consisting of the immune-inducible promoter (Pro_{TBF1}) and two pathogen-responsive upstream open reading frames (uORFs_{TBF1}) of the *Arabidopsis* TBF1 gene. The bars show the mean \pm s.d. ($n = 5$) of the lesion length, and a two-sided Student’s *t* test

was used to determine the significance. **c, d** The flowering phenotype of rice Zhonghua11 (ZH11) plants transformed with Pro_{TBF1}-uORFs_{TBF1}::OsELF3-2-E3TCD1. Two independent transgenic lines (#1 and #2) were used for each construct. The bars show the mean \pm s.d. ($n = 15$) of the days to heading after seeding under the natural long-day (LD) condition, and a two-sided Student’s *t* test was used to determine the significance. **e** The phylogenetic tree to show the homologs of E3TCD1 in *Arabidopsis thaliana* (At), *Oryza sativa* (Os), *Zea mays* (Zm), *Triticum aestivum* (Ta), *Brassica napus* (Bn), and *Solanum lycopersicum* (Sl). Scale bar, 1 cm (**a**), 10 cm (**c**). Source data are provided as a Source Data file.

co-localization assay revealed their ability to co-exist within the condensates (Supplementary Fig. 8c, d). Given these findings, we hypothesized that the OsELF3-1-E3TCD1 or OsELF3-2-E3TCD1 degrader could target OsELF3-1 for degradation based on the design of the TCD system. Subsequently, pilot experiments conducted in *N. benthamiana* indicated that co-expression of OsELF3-1-E3TCD1 or OsELF3-2-E3TCD1 degrader led to a reduction in YFP-OsELF3-1 (Supplementary Fig. 8e, f). Consequently, we observed a significant delay in heading date in transgenic rice lines expressing 35S::OsELF3-1-E3TCD1 or 35S::OsELF3-2-E3TCD1 compared to the control lines 35S::E3TCD1 (Fig. 5c, d). Remarkably, this observation mirrors the phenotype of plants with RNA interference of *OsELF3-1* in the Nipponbare background⁷⁰. These findings in *Arabidopsis* and rice underscore the TCD system in enabling controlled homologous gene functions in a species-specific manner.

Validating the TCD system in modulating rice flowering time

To validate the expression of endogenous *OsELF3-1* in transgenic plants, we conducted experiments using RT-qPCR with different primer pairs. One pair had a primer binding on the 5'-leader, which was not included in the transgene construct, while the other pair was shared by the endogenous *OsELF3-1* and the transgene (Supplementary Fig. 9a). The results revealed that the transgene did not affect the levels of endogenous *OsELF3-1* mRNA, effectively ruling out the possibility of RNA interference with endogenous *OsELF3-1* in the transgenic plants (Supplementary Fig. 9a).

Given the unavailability of an antibody against endogenous OsELF3-1, we employed two complementary methods to assess the transgene’s capability to degrade endogenous OsELF3-1 at the protein level. First, we conducted a semi-in planta assay using rice protoplasts derived from non-transformed ZH11, the control line 35S::E3TCD1, and transgenic plants expressing 35S::OsELF3-1-E3TCD1 or 35S::OsELF3-2-E3TCD1. We introduced 35S::OsELF3-1-YFP constructs alongside

35S::CFP as an internal control. Microscopic observation and immunoblot analysis targeting OsELF3-1-YFP confirmed that the degrader of OsELF3-1-E3TCD1 or OsELF3-2-E3TCD1 effectively degraded the target OsELF3-1 protein (Fig. 5e, f). Moreover, the degradation of OsELF3-1-YFP by the OsELF3-1-E3TCD1 degrader was inhibited upon the addition of TAK-243, as evidenced by the restored fluorescence and immunoblot signals (Supplementary Fig. 8g, h). Second, we measured the mRNA levels of *OsHd1* and *OsGhd7*, whose transcription is repressed by OsELF3-1, as an indirect proxy⁶⁹. Transgenic lines expressing the degrader of OsELF3-1-E3TCD1 or OsELF3-2-E3TCD1 exhibited increased mRNA levels for both *OsHd1* and *OsGhd7* (Supplementary Fig. 9b, c). Together, these results demonstrate that both degraders effectively target endogenous OsELF3-1 protein, the primary homolog regulating flowering in rice.

Conditional TCD in engineering crop defense

In addition to OsELF3-1, our pilot experiments revealed that OsELF3-1-E3TCD1 or OsELF3-2-E3TCD1 degrader could facilitate the degradation of OsELF3-2. This conclusion is supported by microscopic observation and immunoblot analysis conducted in *N. benthamiana* and protoplasts prepared from 35S::OsELF3-1-E3TCD1 and 35S::OsELF3-2-E3TCD1 transgenic plants (Fig. 5e, g and Supplementary Fig. 8e, f). Intriguingly, while OsELF3-1 predominantly regulates flowering, both homologs play a vital role in suppressing resistance to *Magnaporthe oryzae*, the causal agent of rice blast disease^{71,72}. Consequently, transgenic rice lines expressing 35S::OsELF3-1-E3TCD1 and 35S::OsELF3-2-E3TCD1 exhibited reduced disease severity compared to controls (Fig. 6a, b).

To mitigate the pleiotropic effects associated with continuous degradation of OsELF3-1 and OsELF3-2, such as late flowering, we employed the TBF1 cassette to control the TCD system precisely. This cassette allows transcriptional and translational control of target genes by incorporating an immune-inducible promoter (Pro_{TBF1}) and two

pathogen-responsive upstream open reading frames (uORFs_{TBF1}) of the *TBF1* gene^{4,73–75}. Remarkably, transgenic plants with Pro_{TBF1}-uORFs_{TBF1}::OsELF3-2-E3TCD1 showed no alteration in flowering time compared to non-transformed ZH11 plants, indicating stringent control of *OsELF3-2* expression by the TBF1 expression control cassette (Fig. 6c, d). However, these plants exhibited enhanced resistance to *M. oryzae* (Fig. 6a, b). These findings underscore the potential of the TCD system coupled with expression-control elements for conditionally targeted protein degradation, offering practical utility in engineering desirable agronomic traits for genes with pleiotropic effects.

Discussion

Modern agriculture faces many challenges, such as a rapidly growing global population, decreasing arable land, unpredictable climate patterns, and environmental pollution. To foster sustainable agriculture, there's an urgent need for the rapid development of high-yield food and fiber crops resilient to biotic and abiotic stresses. Genetic engineering emerges as a potent tool for swiftly breeding superior cultivars, adept at navigating these challenges by modulating the expression of essential agronomic trait genes across various levels. In this context, we introduce the TCD system, enabling the degradation of endogenous proteins via transgene expression, complementing genetic techniques that manipulate DNA and RNA in plants. These findings will deepen our understanding of protein functionalities in fundamental research and hint at practical applications, potentially as a pivotal transgene strategy for optimizing crop performance.

The success of the TCD system largely depends on identifying an appropriate E3 ligase, referred to as E3TCDs, which can induce self-degradation either independently or when fused with a target protein (X protein). Our study demonstrates the functional efficacy of *Arabidopsis* E3TCD1 in targeting specific TFs for degradation in various expression systems, including *Arabidopsis*, *N. benthamiana*, and rice. Specifically, E3TCD1 successfully degraded 10 out of 12 tested TFs or transcriptional regulators. However, it failed to degrade some TFs despite their similar subcellular localization patterns to the degradable TFs (Supplementary Fig. 3a). This suggests that the X-E3TCD1 in the TCD system might interfere with the recognition of some endogenous TF or the recruitment of other UPS components, resulting in varying degradation efficiencies. Adjusting the conformation between the X protein and E3TCD1 might be beneficial in addressing this issue. In addition, reducing the length of E3TCD1 from its current 666 amino acids may minimize conformational or structural interference. A more promising approach would be to identify additional E3TCDs to broaden the recognition spectrum of the X protein. Although our current study screened candidate E3TCDs from a subset of E3 ligases predicted to be IDPs, we discovered that the primary characteristic of effective E3TCDs is their propensity for self-degradation. We identified numerous E3TCD1 homologs across various plant species (Fig. 6e and Supplementary Data 5). These data suggest the potential for discovering more E3TCDs to expand the substrate recognition spectrum, enhancing the versatility and efficacy of the TCD system. Therefore, a large-scale screening of E3 ligases from various species might be necessary.

The next question concerns the situations where the TCD system could be considered for genetic manipulations. We believe that for genetic analysis with known genes, the TCD system could be applied in scenarios where CRISPR interference (CRISPRi) or RNA interference (RNAi) methods are currently used once the positive results from our pilot experiments. Based on our study of OsELF3-1/2 homologs in rice, the TCD system demonstrates superiority in studying homologous genes with higher identity at the protein level than at the nucleotide level. Unlike CRISPRi or RNAi, which require the expression of multiple gRNAs or RNA fragments to reduce the expression of homologous genes, the TCD system can target and degrade multiple homologs

simultaneously using the TCD with a single gene. For example, in our study, the TCD system effectively reduced the expression of both OsELF3-1 and OsELF3-2 using the TCD with either OsELF3-1 or OsELF3-2, highlighting its efficiency and potential advantages in genetic manipulations involving homologous genes. This advantage may become more pronounced in forward genetic screening, particularly given the widespread occurrence of gene redundancy in plant genomes⁷⁶.

In crop engineering, it's crucial to focus on how to express the transgene within the TCD system. This is important because most genes have multiple functions, leading to potential pleiotropic effects. Therefore, TCD must be precisely regulated to control when, where, and how strongly the gene is expressed. Our study used the TBF1 cassette to control TCD timing, successfully avoiding pleiotropic effects on flowering time caused by OsELF3-1. In addition, adjusting flowering times in rice cultivars could enable rapid adaptation to different light conditions across latitudes. TCD-mediated degradation of OsELF3-1 significantly changed flowering times (Fig. 5c, d). This highlights the possibility of selecting expression intensity to fine-tune flowering time to meet the different requirements of the breeding programs on flowering time. Thus, future research could develop quantitative TCD methods to achieve gradient degradation of specific proteins, resulting in variable phenotypes. This variability could benefit breeding elite cultivars tailored to specific environments, considering factors like light intensity, water availability, temperature fluctuations, and soil composition.

Our study has a limitation in explaining the scale at which TCD works on cleaning condensates away. This is because liquid-liquid phase separation facilitates frequent exchange between the soluble fraction and the condensate. Therefore, TCD may lead to direct degradation of either the condensate or the smaller-sized complex in the soluble fraction continuously exchanged from the condensate. In either scenario, there will be a notable decrease in the amount of the targeted proteins and the corresponding condensates, as observed.

Certain condensates may turn into harmful protein condensates or solidified fiber structures. These harmful condensates have been recently found to compromise plant disease tolerance, and they are associated with neurodegenerative diseases in humans, such as amyotrophic lateral sclerosis (ALS) and Alzheimer's disease^{35,77}. In such cases, the TCD system may effectively eliminate these harmful condensates. Notably, during the peer review of this work, a similar strategy called 'RING-Bait' was reported. This approach combines an aggregating protein sequence with the RING domain of the E3 ubiquitin ligase TRIM21 to specifically degrade tau aggregates, ultimately reducing tau pathology and improving motor function in mice⁷⁸. Another strategy, known as the 'RING-nanobody degrader,' has also been developed. Unlike RING-Bait and our TCD system, this approach fuses the RING domain of TRIM21 to a tau-targeting nanobody, demonstrating the therapeutic potential for tau-associated disorders⁷⁹. Our TCD system targets distinct properties of endogenous proteins, specifically TFs, which are widely linked to various human diseases. As a result, our TCD system holds therapeutic potential for a range of diseases driven by endogenous TFs. Furthermore, our approach begins with de novo mining of unknown E3 ligases, which could help identify E3 candidates suitable for gene therapy in human diseases caused by other types of endogenous proteins. With the rapid advancements in targeted protein degradation strategies^{80–82}, it is exciting to envision their application in plants, where they could significantly accelerate basic research and enhance crop performance, paving the way for an exciting future.

Methods

Plant growth and transformation

All rice lines in this research belong to the *O. sativa* subsp. *japonica* variety Zhonghua 11 (ZH11). Rice plants for phenotypic assessments

were cultivated in the experimental field at Huashan in Wuhan, China (30.3°N, 114.3°E) under natural long-day conditions (LDs). Rice plants for *Magnaporthe oryzae* infection were grown in a greenhouse at 26 °C under a photoperiod of 12 h of light and 12 h of darkness with 90% relative humidity. All *Arabidopsis* lines in this study originate from the Columbia-0 (Col-0) background. *Arabidopsis* and *N. benthamiana* plants were grown in a greenhouse at 23 °C under a photoperiod of 16 h of light and 8 h of darkness with 55% relative humidity. The genetic transformation was performed in the background of ZH11 and Col-0^{28,83}.

Plasmid construction

The full-length coding sequences of *AtELF3* (At2G25930.1) and *E3IDPs* (Supplementary Data 2) were amplified from Col-0 cDNA. The CDSs of *OsTBI* (LOC_Os03g49880.1), *OsELF3-1* (LOC_Os06g05060.1), *OsELF3-2* (LOC_Os01g38530.1), and *OsPLPs* (Supplementary Data 3) were amplified from ZH11 cDNA. All sequences were fused with the indicated N or C terminal tags. All constructs were confirmed through conoly PCR and DNA sequencing. All primers and plasmids are listed in Supplementary Data 6.

Immunoblot analysis

In immunoblot experiments, *N. benthamiana* leaf tissues were collected and ground in liquid nitrogen using a steel bead. Subsequently, 200 µL of lysis buffer (50 mM Tris, pH 7.5, 150 mM NaCl, 0.1% Triton X-100, 0.2% Nonidet P-40, and a protease inhibitor cocktail (Thermo Fisher, Cat#A32955; one tablet per 10 mL) was added to each 100 mg of ground tissue samples. The lysates were incubated at 4 °C for 10 min, followed by centrifugation at 12,000 × *g* to collect the supernatant. Proteins in the supernatant were denatured by adding 1 × SDS-loading buffer and heating at 100 °C for 10 min. The samples were then subjected to Western blotting using anti-GFP (Abclonal, Cat#AE012, Lot#3523030936, dilution: 1:1000) or anti-HA (Abclonal, Cat#AE008, Lot#9200008004, dilution: 1:1000) antibodies.

Transient expression in *N. benthamiana*

We employed *Agrobacterium* strain GV3101 (pMP90) for binary vector delivery. For transient expression in *N. benthamiana*, *Agrobacterium* GV3101 carrying each construct was cultured in LB medium supplemented with kanamycin (50 µg/mL), gentamycin (50 µg/mL), and rifampicin (25 µg/mL) at 28 °C overnight. The agrobacterial cells were resuspended in the infiltration buffer (10 mM 2-(N-morpholino) ethanesulfonic acid, 10 mM MgCl₂, 200 µM acetosyringone) at OD_{600 nm} = 0.1 after centrifugation at 2600 × *g* for 5 min and incubated at room temperature for 1 h.

For microscopic observation in the pilot experiments, *Agrobacterium* containing 35S::CFP and *Agrobacterium* containing 35S::X-YFP or 35S::YFP-X were mixed with *Agrobacterium* containing 35S::E3TCD1 (i.e., E3IDP45) or 35S::X-E3TCD1 (i.e., E3IDP45) at a 1:1:1 ratio. The mixed suspension was infiltrated into three-week-old *N. benthamiana* plants. After 48 h of expression, leaf discs were excised for microscopic observation. CFP and YFP fluorescence were visualized using Leica TCS SP8 upright microscopy, with excitation provided by 448 nm and 514 nm lasers, respectively.

For E3IDP45^{ARING} condensation upon treatments, *N. benthamiana* leaves were infiltrated with *Agrobacterium tumefaciens* harboring the construct 35S::E3IDP45^{ARING}-YFP. After 48 h of incubation, the same leaf regions were subjected to the following treatments: infiltration with 2% 1,6-hexanediol followed by an additional 30 min of incubation, infiltration with 1 mM salicylic acid (SA) followed by an additional 3 h of incubation, infiltration with 500 mM NaCl followed by an additional 1 h of incubation, or exposure to 4 °C or 40 °C for 30 min. After these treatments, leaf discs were excised for microscopic to observe protein condensation.

For the inhibitor treatment assay, proteins from the indicated constructs were transiently expressed in *N. benthamiana* leaves for the indicated time points. Samples were then infiltrated with 10 mM MgCl₂ as the mock control or with 1 µM E1 inhibitor TAK-243, 50 µM proteasome inhibitor MG-132, or 20 µM autophagy inhibitor E64d. For rice protoplasts, following 16 h of transient expression, TAK-243 was added and co-incubated with the protoplasts at a final concentration of 1 µM.

For split luciferase complementation assays, *Agrobacterium* containing the indicated pairwise vectors were mixed at a 1:1 ratio. Negative controls, 35S::HA-nLUC or 35S::nYFP-cLUC, were included. Both the test and control groups were infiltrated into the same leaf of *N. benthamiana* and allowed to express for 48 h. Subsequently, 1 mM luciferin was sprayed onto the leaves, and imaging was conducted using a CCD-camera-equipped box at an exposure time of 20 min under darkness.

For the in vivo analysis of protein degradation in *N. benthamiana*, leaves were infiltrated with *Agrobacterium tumefaciens* harboring the construct 35S::PLP308-YFP. Following a 24-hour incubation period, the same leaf areas were subsequently infiltrated with *Agrobacterium* containing the est::PLP308-E3TCD1 construct. After an additional 24 h of incubation, the leaves were sectioned into three groups and treated with 10 mM MgCl₂, 50 µM β-estradiol, or a combination of 50 µM β-estradiol and 50 µM MG132. Samples were collected at 0, 6, 12, and 24 h post-treatment for immunoblot analysis to quantify PLP308-YFP protein levels. In a parallel experiment, leaves were co-infiltrated with *Agrobacterium* containing 35S::PLP308-YFP and 35S::CFP. These leaves were then infiltrated with *Agrobacterium* harboring the est::PLP308-E3TCD1 construct, followed by treatment with 50 µM β-estradiol as described. Leaf samples were collected at 0 and 12 h post-treatment for fluorescence microscopy to observe protein localization and degradation.

For co-immunoprecipitation (co-IP) analysis in *N. benthamiana*, *Agrobacterium* containing 35S::YFP-OsELF3-1 was mixed in equal amounts with *Agrobacterium* containing 35S::HA-OsELF3-2 or 35S::HA-nLUC. The mixed suspension was infiltrated into three-week-old *N. benthamiana* plants. After 48 h of expression, 1 g of leaf tissue was collected from each sample for protein extraction. From the 2 mL of total extracted protein, 90 µL was taken as input, and the remaining protein was incubated with 100 µL GFP-Trap A beads on a rotating shaker for 1 h at 4 °C. The beads were then collected using a magnetic separator, the supernatant was discarded, and the beads were washed with 1 mL of washing buffer (50 mM Tris, pH 7.5, 150 mM NaCl, 1 mM PMSF) for 1 min. This washing step was repeated three times, after which the supernatant was discarded. Finally, the bead-bound proteins were mixed with 100 µL of 1 × SDS-loading buffer, and the 90 µL input samples were mixed with 10 µL of 10 × SDS-loading buffer. Both sets of samples were then heated at 100 °C for 10 min. Subsequently, the samples were subjected to immunoblot analysis.

Pathogen infection

Isolates of *Magnaporthe oryzae* strain RB22 were incubated on an oatmeal medium (3% [w/v] oats and 1.5% [w/v] agar). The cultures were incubated at 26 °C under low light conditions for 18 days. Following incubation, spores were harvested by washing the plates with a small volume of 0.1% (v/v) Tween 20. The spore suspensions were subsequently filtered through Miracloth and diluted with 0.1% (v/v) Tween 20 to achieve a final concentration of 5.0 × 10⁵ spores/mL. For the infection assay, wounds were created on the abaxial surface of rice leaves. A 10 µL aliquot of the spore suspension was subsequently applied to each wound site. The inoculated leaves were then covered with cellophane tape to maintain humidity. After a ten-day incubation period, disease severity was assessed by measuring the length of the lesions on the rice leaves.

In vitro phase separation assay

The MBP-YFP-E3IDP45 MBP-YFP-OsELF3-1, MBP-YFP-OsELF3-1-E3TCD1 and MBP-CFP-LCD_{HEMI} fusion protein was expressed in *E. coli* (DE3) cells²⁷. Post cell lysis and purification, the MBP tag was enzymatically cleaved using 10 µg/mL Xa factor protease (NEB, Cat#P8010) at 23 °C overnight. To induce phase separation, PEG8000 (Sigma, Cat#25322-68-3) was added to the indicated final concentrations. Proteins, either with or without the MBP tag were then coated onto confocal flat dishes and observed using a Leica TCS SP8 upright microscope equipped with a 10 × objective lens and a 514 nm laser for excitation. FRAP was performed by bleaching the region of interest with a 514 nm laser at 80% power intensity, applied twice. The recovery of YFP fluorescence was monitored at intervals of 1.3 s post-bleaching. To dissolve the condensates, a final concentration of 10% 1,6-hexanediol or 500 mM NaCl was applied, and the samples were subsequently analyzed using microscopy.

Transient expression in the rice protoplast

To transiently express genes in rice protoplasts, dehulled rice seeds were disinfected using a 2% hypochlorous acid solution. The disinfected seeds were then planted on 1/2 MS medium and incubated in a light chamber at 28 °C under a photoperiod of 14 h of light and 10 h of darkness with 60% relative humidity. After 14 days, approximately 40 uniformly grown seedlings were selected, and seedling stems were excised into small segments approximately 1 mm in length. These segments were incubated in 20 mL of enzyme solution (1.5% Cellulose RS (Yacult Pharmaceutical), 0.75% Macerozyme R-10 (Yacult Pharmaceutical), 0.6 M Mannitol, 1 mM CaCl₂, 0.1% BSA, 10 mM MES (pH 5.7)) on a rotary shaker at 40 rpm and 25 °C for 5 h to facilitate enzymatic digestion. The resulting digestion mixture was filtered through a 40 µm nylon mesh to eliminate plant debris. Protoplasts were harvested by centrifugation at 100 × g, and the supernatant was discarded. The protoplasts were subsequently washed with W5 solution (154 mM NaCl, 5 mM KCl, 125 mM CaCl₂, and 2 mM MES, pH 5.7) and resuspended in MMG solution (0.6 M mannitol, 15 mM MgCl₂, and 4 mM MES, pH 5.7) at a concentration of 1 × 10⁷ cells/mL. For transformation, 5 µg of the desired plasmid was added to 100 µL of the protoplast suspension, followed by incubation with an equal volume of PEG-CaCl₂ solution (0.6 M mannitol, 100 mM CaCl₂, and 40% PEG4000) for 15 min. The reaction was terminated by the addition of 1 mL W5 solution, and the protoplasts were collected by centrifugation at 100 × g. The transformed protoplasts were then transferred to 1 mL WI solution (0.6 M mannitol, 4 mM KCl, and 4 mM MES, pH 5.7) and incubated in the dark at 28 °C for 16 h. Following the incubation period, the protoplasts were subjected to microscopic observation and protein extraction.

Semi-in vivo protein degradation assay

In the semi-in vivo protein degradation assay, 5 µg of the 35S::CFP plasmid was combined with 5 µg of either the 35S::YFP-OsELF3-1 or 35S::YFP-OsELF3-2 plasmid. These plasmid mixtures were subsequently introduced into 100 µL of rice protoplasts. The protoplasts were isolated from non-transformed ZH11, control line 35S::E3TCD1, and transgenic lines expressing 35S::OsELF3-1-E3TCD1#1 or 35S::OsELF3-2-E3TCD1#1. Following a 16-hour transformation period, the protoplasts were subjected to confocal microscopy and immunoblot analysis.

In vitro ubiquitylation assay

For the in vitro ubiquitylation assay, fusion proteins His-E1 (AtUBA1), His-E2 (AtUBC8), His-Ub (AtUBQ10), MBP-E3IDP45, MBP-E3IDP45^{ΔCD}, MBP-E3TCD1-PLP308, and MBP-HA-PLP308 were expressed in *E. coli* (DE3) cells, followed by cell lysis and His tag-based purification. To assess self-ubiquitylation of E3IDP45 or E3IDP45^{ΔCD}, 1 µg of His-E1, 1 µg of His-E2, 1 µg of MBP-E3IDP45 or MBP-E3IDP45^{ΔCD}, and 1 µg of

His-Ub were combined in 30 µL of ubiquitylation reaction buffer (20 mM Tris-HCl, pH 7.5, 5 mM MgCl₂, 0.5 mM DTT, and 2 mM ATP). The reaction was incubated at 24 °C for 8 h. The products were analyzed by immunoblotting with anti-MBP (Abclonal, Cat#AE016, Lot#9200016002, dilution: 1:1000). To examine substrate ubiquitylation, 1 µg of His-E1, 1 µg of His-E2, 1 µg of MBP-E3TCD1-PLP308, 1 µg of MBP-HA-PLP308, and 1 µg of His-Ub were dissolved in 30 µL of the same ubiquitylation reaction buffer under identical conditions. Reaction products were analyzed by immunoblotting with anti-HA (Abclonal, Cat#AE008, Lot#9200008004, dilution: 1:1000). For secondary immunoblotting to detect ubiquitin, the membrane was incubated in stripping buffer (20 mM Tris-HCl, pH 2.0, 1% SDS) for 20 min to remove bound antibodies. After washing with PBS (137 mM NaCl, 2.7 mM KCl, 15 mM Na₂HPO₄, 4.4 mM KH₂PO₄) three times for 30 min, the membrane was re-probed with anti-Ub (Cell Signaling, Cat#3936; Lot#19, dilution: 1:1000) antibodies to detect ubiquitin conjugates.

RT-qPCR and RT-PCR

Total RNA was isolated from 100 mg of leaf tissue using 1 mL of TRIzol (Vazyme, Cat#R401-01) following the manufacturer's instructions. Subsequently, reverse transcription was carried out using the HiScript III 1st Strand cDNA Synthesis Kit (Vazyme, Cat#R312-01). Real-time quantitative PCR (qPCR) assays were performed using Taq Pro Universal SYBR qPCR Master Mix (Vazyme, Cat#Q712-02). *OsActin1* was utilized as the internal control for rice. RT-PCR was conducted using Phanta Max Super-Fidelity DNA Polymerase (Vazyme, Cat#P505-d1). In experiments involving rice protoplasts and *N. benthamiana*, *OsUbiquitin* (*OsUBQ*, LOC_Os03g13170) and *NbUbiquitin* (*NbUBQ*, AY912494) served as internal controls, respectively. Detailed information on primers and plasmids can be found in Supplementary Data 6.

IDP prediction

To predict intrinsically disordered proteins (IDPs), the amino acid sequences were submitted to [PLAAC](#) with default parameters, using the *Arabidopsis* proteome as the background. Amino acid stretches with HMMPrD-like scores exceeding 0.5 for at least 10 consecutive residues were identified as Prion-like domains (PrD-like domains). Proteins containing at least one such domain were classified as IDPs. Additionally, the sequences were analyzed using D²P² (<https://d2p2.pro/>), SMART, and MolPhase (<https://molphase.sbs.ntu.edu.sg/>) for further predictions. Detailed information on the predicted proteins is provided in Supplementary Data 1.

Phylogenetic tree analysis

Phylogenetic analysis was conducted using diverse species, including *Arabidopsis thaliana*, *Oryza sativa*, *Zea mays*, *Triticum aestivum*, *Brassica napus*, and *Solanum lycopersicum*. Predicted ELF3 protein sequences were retrieved from the Plant orthologs of AtELF3 in TAIR (<https://www.arabidopsis.org/>), while predicted E3IDP45 protein sequences were obtained from the Protein BLAST tool available on the National Center for Biotechnology Information (NCBI) database (<https://www.ncbi.nlm.nih.gov/>). The BLAST search was performed using default parameters. Detailed information on predicted protein can be found in Supplementary Data 5. For the construction of the phylogenetic tree, each protein sequence was aligned using ClustalW. Subsequently, 1000 bootstrap replicates were generated for evolutionary analysis using the Neighbor-Joining method. These analyses were carried out using MAGA11⁸⁴.

Statistical methods

Our comprehensive analysis employed rigorous statistical methodologies using GraphPad Prism 8 or RStudio. We assumed a normal distribution for parametric statistics when the Shapiro-Wilk test yielded a *P*-value greater than 0.05. For comparisons between the two groups, we used a two-sided Student's *t* test. E3 screening and

in vitro phase separation experiments have only been performed once. Unless stated otherwise, “n” represents biological replicates, and all experiments were conducted independently at least twice. Additional statistical parameters are outlined in the Figure legends for further elucidation.

Reporting summary

Further information on research design is available in the Nature Portfolio Reporting Summary linked to this article.

Data availability

All materials are available from the corresponding author upon request. All data generated in this study are provided in this article and its Supplementary Information file. Source data are provided in this paper.

References

- Bailey-Serres, J., Parker, J. E., Ainsworth, E. A., Oldroyd, G. E. D. & Schroeder, J. I. Genetic strategies for improving crop yields. *Nature* **575**, 109–118 (2019).
- Liu, G., Lin, Q., Jin, S. & Gao, C. The CRISPR-Cas toolbox and gene editing technologies. *Mol. Cell* **82**, 333–347 (2022).
- Cardi, T. et al. CRISPR/Cas-mediated plant genome editing: outstanding challenges a decade after implementation. *Trends Plant Sci.* **28**, 1144–1165 (2023).
- Mou, R., Niu, R., Yang, R. & Xu, G. Engineering crop performance with upstream open reading frames. *Trends Plant Sci.* <https://doi.org/10.1016/j.tplants.2024.10.005> (2024).
- Kamthan, A., Chaudhuri, A., Kamthan, M. & Datta, A. Small RNAs in plants: recent development and application for crop improvement. *Front. Plant Sci.* **6**, <https://doi.org/10.3389/fpls.2015.00208> (2015).
- Xu, G. et al. One-step, zero-background ligation-independent cloning intron-containing hairpin RNA constructs for RNAi in plants. *New Phytol.* **187**, 240–250 (2010).
- Solis-Miranda, J. et al. Stress-related biomolecular condensates in plants. *Plant Cell* **35**, 3187–3204 (2023).
- Maruri-Lopez, I. & Chodasiewicz, M. Involvement of small molecules and metabolites in regulation of biomolecular condensate properties. *Curr. Opin. Plant Biol.* **74**, 102385 (2023).
- Hatzianestis, I. H., Mountourakis, F., Stavridou, S. & Moschou, P. N. Plant condensates: no longer membrane-less? *Trends Plant Sci.* **28**, 1101–1112 (2023).
- Garcia-Cabau, C. & Salvatella, X. Regulation of biomolecular condensate dynamics by signaling. *Curr. Opin. Cell Biol.* **69**, 111–119 (2021).
- Cuevas-Velazquez, C. L. & Dinneny, J. R. Organization out of disorder: liquid-liquid phase separation in plants. *Curr. Opin. Plant Biol.* **45**, 68–74 (2018).
- Wang, W. & Gu, Y. The emerging role of biomolecular condensates in plant immunity. *Plant Cell* **34**, 1568–1572 (2022).
- Fang, X. & Li, P. Snapshot: condensates in plant biology. *Cell* **187**, 2894–2894 (2024).
- Huang, S., Zhu, S., Kumar, P. & MacMicking, J. D. A phase-separated nuclear GBPL circuit controls immunity in plants. *Nature* **594**, 424–429 (2021).
- Zavaliev, R., Mohan, R., Chen, T. & Dong, X. Formation of NPR1 condensates promotes cell survival during the plant immune response. *Cell* **182**, 1093–1108 (2020).
- Jung, J.-H. et al. A prion-like domain in ELF3 functions as a thermosensor in Arabidopsis. *Nature* **585**, 256–260 (2020).
- Fang, X. et al. Arabidopsis FLL2 promotes liquid-liquid phase separation of polyadenylation complexes. *Nature* **569**, 265–269 (2019).
- Powers, S. K. et al. Nucleo-cytoplasmic partitioning of ARF proteins controls auxin responses in *Arabidopsis thaliana*. *Mol. Cell* **76**, 177–190 (2019).
- Freeman Rosenzweig, E. S. et al. The eukaryotic CO₂-concentrating organelle is liquid-like and exhibits dynamic reorganization. *Cell* **171**, 148–162 (2017).
- Ouyang, M. et al. Liquid-liquid phase transition drives intra-chloroplast cargo sorting. *Cell* **180**, 1144–1159 (2020).
- Zhang, Y., Li, Z., Chen, N., Huang, Y. & Huang, S. Phase separation of Arabidopsis EMB1579 controls transcription, mRNA splicing, and development. *PLoS Biol.* **18**, e3000782 (2020).
- Dorone, Y. et al. A prion-like protein regulator of seed germination undergoes hydration-dependent phase separation. *Cell* **184**, 4284–4298 (2021).
- Huang, X. et al. ROS regulated reversible protein phase separation synchronizes plant flowering. *Nat. Chem. Biol.* **17**, 549–557 (2021).
- Song, P. et al. Arabidopsis N⁶-methyladenosine reader CPSF30-L recognizes FUE signals to control polyadenylation site choice in liquid-like nuclear bodies. *Mol. Plant* **14**, 571–587 (2021).
- Xie, D. et al. Phase separation of SERRATE drives dicing body assembly and promotes miRNA processing in Arabidopsis. *Nat. Cell Biol.* **23**, 32–39 (2021).
- Zhou, G. et al. Proximity editing to identify RNAs in phase-separated RNA binding protein condensates. *Cell Discov.* **7**, 72 (2021).
- Xie, Z. et al. Phenolic acid-induced phase separation and translation inhibition mediate plant interspecific competition. *Nat. Plants* **9**, 1481–1499 (2023).
- Zhou, Y. et al. Plant HEM1 specifies a condensation domain to control immune gene translation. *Nat. Plants* **9**, 289–301 (2023).
- Wang, H. et al. ECT9 condensates with ECT1 and regulates plant immunity. *Front. Plant Sci.* **14**, 1140840 (2023).
- Jia, M., Chen, X., Shi, X., Fang, Y. & Gu, Y. Nuclear transport receptor KA120 regulates molecular condensation of MAC3 to coordinate plant immune activation. *Cell Host Microbe* **31**, 1685–1699 (2023).
- Huang, X. Z. et al. Heterotypic transcriptional condensates formed by prion-like paralogous proteins canalize flowering transition in tomato. *Genome Biol.* **23**, 78 (2022).
- Kim, J. H. et al. Increasing the resilience of plant immunity to a warming climate. *Nature* **607**, 339–344 (2022).
- Zhu, S. et al. Liquid-liquid phase separation of RBGD2/4 is required for heat stress resistance in Arabidopsis. *Dev. Cell* **57**, 583–597 (2022).
- Wu, X. et al. N⁶-methyladenosine-mediated feedback regulation of abscisic acid perception via phase-separated ECT8 condensates in Arabidopsis. *Nat. Plants* **10**, 469–482 (2024).
- Tang, Z. et al. Alleviating protein-condensation-associated damage at the endoplasmic reticulum enhances plant disease tolerance. *Cell Host Microbe* (2024).
- Liu, Y. & Bassham, D. C. Autophagy: pathways for self-eating in plant cells. *Annu. Rev. Plant Biol.* **63**, 215–237 (2012).
- Raffener, M., Zhu, S., González-Fuente, M. & Üstün, S. Interplay between autophagy and proteasome during protein turnover. *Trends Plant Sci.* **28**, 698–714 (2023).
- Eckardt, N. A. et al. The lowdown on breakdown: Open questions in plant proteolysis. *Plant Cell* (2024).
- Zheng, N. & Shabek, N. Ubiquitin ligases: Structure, function, and regulation. *Annu. Rev. Biochem.* **86**, 129–157 (2017).
- Klionsky, D. J. et al. Guidelines for the use and interpretation of assays for monitoring autophagy (4th edition)1. *Autophagy* **17**, 1–382 (2021).
- Wu, T. et al. Targeted protein degradation as a powerful research tool in basic biology and drug target discovery. *Nat. Struct. Mol. Biol.* **27**, 605–614 (2020).

42. Takahashi, D. et al. AUTACs: cargo-specific degraders using selective autophagy. *Mol. Cell* **76**, 797–810 (2019).
43. Nishimura, K., Fukagawa, T., Takisawa, H., Kakimoto, T. & Kanemaki, M. An auxin-based degron system for the rapid depletion of proteins in nonplant cells. *Nat. Methods* **6**, 917–922 (2009).
44. Tsai, J. M., Nowak, R. P., Ebert, B. L. & Fischer, E. S. Targeted protein degradation: from mechanisms to clinic. *Nat. Rev. Mol. Cell Biol.* **25**, 740–757 (2024).
45. Su, L., Li, A., Li, H., Chu, C. & Qiu, J.-L. Direct modulation of protein level in arabidopsis. *Mol. Plant* **6**, 1711–1714 (2013).
46. Faden, F. et al. Phenotypes on demand via switchable target protein degradation in multicellular organisms. *Nat. Commun.* **7**, 12202 (2016).
47. Baudisch, B., Pfort, I., Sorge, E. & Conrad, U. Nanobody-directed specific degradation of proteins by the 26S-proteasome in plants. *Front. Plant Sci.* **9**, <https://doi.org/10.3389/fpls.2018.00130> (2018).
48. Ma, Y. et al. WUSCHEL acts as an auxin response rheostat to maintain apical stem cells in Arabidopsis. *Nat. Commun.* **10**, 5093 (2019).
49. Caussinus, E., Kanca, O. & Affolter, M. Fluorescent fusion protein knockout mediated by anti-GFP nanobody. *Nat. Struct. Mol. Biol.* **19**, 117–121 (2012).
50. Huang, L. & Rojas-Pierce, M. Rapid depletion of target proteins in plants by an inducible protein degradation system. *Plant Cell* **36**, 3145–3161 (2024).
51. Abyzov, A., Blackledge, M. & Zweckstetter, M. Conformational dynamics of intrinsically disordered proteins regulate biomolecular condensate chemistry. *Chem. Rev.* **122**, 6719–6748 (2022).
52. Alberti, S., Gladfelter, A. & Mittag, T. Considerations and challenges in studying liquid-liquid phase separation and biomolecular condensates. *Cell* **176**, 419–434 (2019).
53. Jiménez-López, D., Muñoz-Belman, F., González-Prieto, J. M., Aguilar-Hernández, V. & Guzmán, P. Repertoire of plant RING E3 ubiquitin ligases revisited: new groups counting gene families and single genes. *PLoS ONE* **13**, e0203442 (2018).
54. Chen, L. & Hellmann, H. Plant E3 ligases: flexible enzymes in a sessile world. *Mol. Plant* **6**, 1388–1404 (2013).
55. Lancaster, A. K., Nutter-Upham, A., Lindquist, S. & King, O. D. PLAAC: a web and command-line application to identify proteins with prion-like amino acid composition. *Bioinformatics* **30**, 2501–2502 (2014).
56. Liang, Q. et al. MolPhase, an advanced prediction algorithm for protein phase separation. *EMBO J.* **43**, 1898–1918 (2024).
57. Powers, S. K. et al. Nucleo-cytoplasmic partitioning of ARF proteins controls auxin responses in. *Mol. Cell* **76**, 177–190 (2019).
58. Wagh, K., Garcia, D. A. & Upadhyaya, A. Phase separation in transcription factor dynamics and chromatin organization. *Curr. Opin. Struct. Biol.* **71**, 148–155 (2021).
59. Jin, J. et al. PlantTFDB 4.0: toward a central hub for transcription factors and regulatory interactions in plants. *Nucleic Acids Res.* **45**, D1040–D1045 (2017).
60. Cheng, S. L. H. et al. Nutrient status regulates MED19a phase separation for ORESARA1-dependent senescence. *New Phytol.* **236**, 1779–1795 (2022).
61. Boija, A. et al. Transcription factors activate genes through the phase-separation capacity of their activation domains. *Cell* **175**, 1842–1855 (2018).
62. Lee, H. et al. The Arabidopsis HOS1 gene negatively regulates cold signal transduction and encodes a RING finger protein that displays cold-regulated nucleo-cytoplasmic partitioning. *Genes Dev.* **15**, 912–924 (2001).
63. Takeda, T. et al. The OsTB1 gene negatively regulates lateral branching in rice. *Plant J.* **33**, 513–520 (2003).
64. Choi, M. S. et al. Teosinte Branched 1 modulates tillering in rice plants. *Plant Cell Rep.* **31**, 57–65 (2012).
65. Guo, S. Y. et al. The interaction between OsMADS57 and OsTB1 modulates rice tillering via DWARF14. *Nat. Commun.* **4**, 1566 (2013).
66. Lyu, J. et al. Neo-functionalization of a teosinte branched 1 homologue mediates adaptations of upland rice. *Nat. Commun.* **11**, 725 (2020).
67. Nusinow, D. A. et al. The ELF4-ELF3-LUX complex links the circadian clock to diurnal control of hypocotyl growth. *Nature* **475**, 398–U161 (2011).
68. Fu, C. et al. OsEF3, a homologous gene of Arabidopsis ELF3, has pleiotropic effects in rice. *Plant Biol.* **11**, 751–757 (2009).
69. Yang, Y., Peng, Q., Chen, G.-X., Li, X.-H. & Wu, C.-Y. OsELF3 is involved in circadian clock regulation for promoting flowering under long-day conditions in rice. *Mol. Plant* **6**, 202–215 (2013).
70. Zhao, J. et al. OsELF3-1, an ortholog of Arabidopsis EARLY FLOWERING 3, regulates rice circadian rhythm and photoperiodic flowering. *PLoS ONE* **7**, e43705 (2012).
71. Yi, H. et al. E3 ubiquitin ligase IPI1 controls rice immunity and flowering via both E3 ligase-dependent and -independent pathways. *Dev. Cell* (2024).
72. Xu, X. et al. A pair of E3 ubiquitin ligases control immunity and flowering by targeting different ELF3 proteins in rice. *Dev. Cell* (2024).
73. Xu, G. et al. Global translational reprogramming is a fundamental layer of immune regulation in plants. *Nature* **545**, 487–490 (2017).
74. Xu, G. et al. uORF-mediated translation allows engineered plant disease resistance without fitness costs. *Nature* **545**, 491–494 (2017).
75. Yuan, S., Zhou, G. & Xu, G. Translation machinery: the basis of translational control. *J. Genet. Genom.* <https://doi.org/10.1016/j.jgg.2023.07.009> (2023).
76. Iohannes, S. D. & Jackson, D. Tackling redundancy: genetic mechanisms underlying paralogue compensation in plants. *New Phytol.* **240**, 1381–1389 (2023).
77. Long, J. M. & Holtzman, D. M. Alzheimer disease: an update on pathobiology and treatment strategies. *Cell* **179**, 312–339 (2019).
78. Miller, L. V. C. et al. Co-opting templated aggregation to degrade pathogenic tau assemblies and improve motor function. *Cell* **187**, 5967–5980 (2024).
79. Benn, J. et al. Aggregate-selective removal of pathological tau by clustering-activated degraders. *Science* **385**, 1009–1016 (2024).
80. Zhang, D. et al. Transferrin receptor targeting chimeras for membrane protein degradation. *Nature* <https://doi.org/10.1038/s41586-024-07947-3> (2024).
81. Lu, P. et al. Selective degradation of multimeric proteins by TRIM21-based molecular glue and PROTAC degraders. *Cell* **187**, 7126–7142 (2024).
82. Li, Z. et al. Allele-selective lowering of mutant HTT protein by HTT-LC3 linker compounds. *Nature* **575**, 203–209 (2019).
83. Tian, J. et al. Engineering disease-resistant plants with alternative translation efficiency by switching uORF types through CRISPR. *Sci. China Life Sci.* **67**, 1715–1726 (2024).
84. Tamura, K., Stecher, G. & Kumar, S. MEGA11: molecular evolutionary genetics analysis version 11. *Mol. Biol. Evol.* **38**, 3022–3027 (2021).

Acknowledgements

This study was supported by grants from the Biological Breeding-National Science and Technology Major Project (2023ZD04073) to G.X., the National Natural Science Foundation of China (32470282), the Major Project of Hubei Hongshan Laboratory (2022hszd016) and the Key Research and Development Program of Hubei Province (2022BFE003) to G.X.

Author contributions

G.X. and M.L. designed the experiment. M.L., S.Z., R.N., and G.X. analyzed the data and prepared the figures. S.Z. and R.N. performed all bioinformatics analyses. M.L. performed the experiments with the help of Q.W., H.D., J.L., and Z.Wang. Y.T., Y.N., and M.Y. helped with data analysis. G.X. and M.L. wrote the manuscript with input from all authors.

Competing interests

A patent with the application number 2024116014154 using all data generated from this study has been filed by Wuhan University, listing G.X., M.L., and Q.W. as inventors. Other authors claim no competing interests.

Additional information

Supplementary information The online version contains supplementary material available at <https://doi.org/10.1038/s41467-025-56570-x>.

Correspondence and requests for materials should be addressed to Guoyong Xu.

Peer review information *Nature Communications* thanks Panagiotis Moschou, and the other anonymous reviewer(s) for their contribution to the peer review of this work. A peer review file is available.

Reprints and permissions information is available at <http://www.nature.com/reprints>

Publisher's note Springer Nature remains neutral with regard to jurisdictional claims in published maps and institutional affiliations.

Open Access This article is licensed under a Creative Commons Attribution-NonCommercial-NoDerivatives 4.0 International License, which permits any non-commercial use, sharing, distribution and reproduction in any medium or format, as long as you give appropriate credit to the original author(s) and the source, provide a link to the Creative Commons licence, and indicate if you modified the licensed material. You do not have permission under this licence to share adapted material derived from this article or parts of it. The images or other third party material in this article are included in the article's Creative Commons licence, unless indicated otherwise in a credit line to the material. If material is not included in the article's Creative Commons licence and your intended use is not permitted by statutory regulation or exceeds the permitted use, you will need to obtain permission directly from the copyright holder. To view a copy of this licence, visit <http://creativecommons.org/licenses/by-nc-nd/4.0/>.

© The Author(s) 2025